communications physics

A Nature Portfolio journal

Article

https://doi.org/10.1038/s42005-025-02010-7

Achievement of a vacuum-levitated metal mechanical oscillator with ultra-low damping rate at room temperature

Fang Xiong[1], Leilei Guo[1], Zhiming Chen[1], Aimin Du[2], Cuihong Li[1] ✉ & Tong Wu[1] ✉

A vacuum-levitated metal mechanical oscillator with an ultra-low damping rate is an ideal tool for detecting mass-related short-range forces; however, its realization at room temperature has not yet been achieved, limiting its practical applications. In this study, we developed such an oscillator using a diamagnetically levitated bismuth sphere. We derived an accurate general formula for the sphere's eddy current damping rate and, based on this, constructed the oscillator from microparticles, successfully reducing its damping rate experimentally to $(144 \pm 6)\,\mu$Hz—nearly three orders of magnitude lower than that of the untreated sphere. This improvement allows the sub-millimeter-sized levitated metal mechanical oscillator to theoretically achieve a force sensitivity of $(5.17 \pm 0.12)\ \mathrm{fN}/\sqrt{\mathrm{Hz}}$ and an acceleration sensitivity of $(0.30 \pm 0.01)\ \mathrm{ng}/\sqrt{\mathrm{Hz}}$ at room temperature. Calculations indicate that using this sphere as a test mass can detect gravitational forces from sub-milligram sources, highlighting its potential for short-range force sensing and the exploration of quantum gravity.

Short-range force measurements are crucial for advancing fundamental physics[1–3], frontier physics[4–6], and chemical physics[7]. These forces are inherently weak, requiring the use of highly sensitive test masses for accurate detection. Metal mechanical oscillators have been extensively employed as test masses in numerous short-range force experiments[2,8–16], especially in studies involving small-scale gravitational interactions[2,11–13], the Casimir force[8–10], and searches for hypothetical fifth forces beyond the Standard Model[14,15]. The choice of metal oscillators is motivated by two primary advantages. First, the high density nature of metals enhances force signals within the limited spatial detection range of short-range force experiments, as many of these forces are mass-related[2,12,13]. Second, in short-range experiments where electromagnetic forces often pose challenges, the low electrical work function of metals minimizes charge accumulation, thereby mitigating electromagnetic interference[8,10,12].

For mass-related short-range force detection, great efforts have been made to enhance the sensitivity of these metal mechanical oscillators by mounting metal test masses onto various high-quality mechanical systems, such as cantilever[17–19] and torsion balance[12,20–23]. While these approaches have yielded significant advancements[12,18,19], clamping-induced dissipation remains a limiting factor. This has motivated the exploration of vacuum-levitated mechanical systems[24–26], which eliminate environmental contact dissipation and significantly enhance detection sensitivity to force[27,28] and acceleration[29–33]. However, levitating massive metal mechanical oscillators, essential for certain short-range force detection experiments, remains challenging for most levitation systems[34,35]. Currently, only superconducting and diamagnetic levitation systems can levitate such massive metal mechanical oscillators[36–38]. Although superconducting levitation systems are highly sensitive, they are operated in environments susceptible to electromagnetic heating and vibrations, which can destabilize the superconducting state, particularly when driving force sources at close proximity[13,39,40]. This instability might limit their practical application in short-range force detection experiments. In contrast, while the diamagnetic levitation system is more effective at manipulating close-proximity force sources[41], it is limited to levitating only a few metals with exceptionally high diamagnetic susceptibility, such as bismuth and antimony[36,38]. Reports on diamagnetically levitated metal oscillators at room temperature are scarce. Furthermore, eddy current damping would pose a significant challenge, greatly limiting the sensitivity of the diamagnetic levitation system[41–43]. Existing studies have used pyrolytic graphite powder to fabricate levitated composite pyrolytic graphite plates as a means to reduce eddy current damping rate[42,44]. However, there have been no reports to date on vacuum-levitated high-density spherical metal oscillators.

Here we derive an accurate general formula for the eddy current damping rate of a diamagnetically levitated metal sphere. Based on this formula, we propose and experimentally demonstrate a bismuth sphere

[1]Frontier Fundamental Research Center, Zhejiang Lab, Hangzhou, China. [2]CAS Engineering Laboratory for Deep Resources Equipment and Technology, Institute of Geology and Geophysics, Chinese Academy of Sciences, Beijing, China. ✉e-mail: licuihong@zhejianglab.org; wutong@zhejianglab.org

constructed from microparticles (BM sphere), which reduces the eddy current damping rate by three orders of magnitude compared to a monolithic bismuth sphere. This ultralow eddy current damping rate and high-density nature enable the development of a vacuum diamagnetically levitated BM sphere mechanical oscillator system with ultrahigh sensitivity. The BM sphere's diameters range from a few micrometers to millimeters, covering the size range relevant for short-range force detection. Our experimental results indicate that the eddy current damping rate is reduced to $(144 \pm 6)\,\mu$Hz. From these results, we obtained the necessary parameters for calculating sensitivity. Based on these parameters, we theoretically determined that a sub-millimeter-sized BM sphere can achieve a force sensitivity of (5.17 ± 0.12) fN$/\sqrt{\text{Hz}}$ and an acceleration sensitivity of (0.30 ± 0.01) ng$/\sqrt{\text{Hz}}$ at room temperature. Our calculations demonstrate that, with a measurement time around 2500 s, this system can detect gravitational force from a 0.9 mg gravitational mass. In contrast, the current smallest detectable gravitational mass is 90 mg, as achieved by a Cavendish torsion balance scheme[12]. This study validates a diamagnetically levitated BM sphere mechanical oscillator with high force and acceleration sensitivities, offering promising applications in short-range force detection, testing new physics, and exploring quantum gravity.

Results

Theoretical model

For a diamagnetically levitated metal mechanical oscillator, motion in the presence of a magnetic field induces eddy current damping, leading to energy dissipation. According to the fluctuation-dissipation theorem, this dissipation is accompanied by fluctuating current white noise, also known as Johnson-Nyquist noise. This noise produces Lorentz force fluctuations in the magnetic field, which ultimately affect the force and acceleration sensitivity of the oscillator. Our theoretical derivations (See Supplementary Note 1) indicate that the force and acceleration sensitivities are given by:

$$\sqrt{S_{FF}} = \sqrt{4m\gamma k_B T}, \quad \sqrt{S_{aa}} = \sqrt{\frac{4\gamma k_B T}{m}}, \tag{1}$$

where γ is the mechanical damping rate, which consists of two primary components: the eddy current damping rate and the air damping rate due to collisions with air molecules. k_B is Boltzmann's constant, T is the temperature, and m is the mass of the mechanical oscillator. In vacuum environments, eddy current damping typically dominates over air damping, making the reduction of eddy current damping crucial for enhancing the force and acceleration sensitivity of metal mechanical oscillators.

Deriving an analytical expression for the eddy current damping rate is essential for guiding experimental efforts to minimize it. While numerical solutions can be obtained by numerically solving Maxwell's equations, an analytical solution remains challenging due to the complex magnetic field distribution and particle geometry. Furthermore, existing analytical models for eddy current damping are not applicable to levitation systems[42,43]. In this study, we present a general analytical expression to quantify the eddy current damping rate of any diamagnetically levitated metal sphere. The detailed derivation is outlined in Supplementary Note 2, and it leads to the formulation of the damping force on a sphere as:

$$\boldsymbol{F} = -m\overleftrightarrow{\gamma}\boldsymbol{v}, \tag{2}$$

where $\overleftrightarrow{\gamma}$ is a second-order damping tensor. Expanding this expression gives:

$$\begin{bmatrix} F_x \\ F_y \\ F_z \end{bmatrix} = -m \begin{bmatrix} \gamma_{xx} & \gamma_{xy} & \gamma_{xz} \\ \gamma_{yx} & \gamma_{yy} & \gamma_{yz} \\ \gamma_{zx} & \gamma_{zy} & \gamma_{zz} \end{bmatrix} \begin{bmatrix} v_x \\ v_y \\ v_z \end{bmatrix} \tag{3}$$

Each element of the damping tensor is expressed as:

$$\gamma_{ij} = \frac{2\pi}{15m}\sigma R^5 \sum_n \frac{\partial B_n}{\partial i}\frac{\partial B_n}{\partial j}, \quad (i,j,n = x,y,z), \tag{4}$$

where m is the particle mass, R is the sphere radius, σ is the electrical conductivity, and B_n is the magnetic flux density in the n-direction at the sphere's location. At the levitation position, $\frac{\partial B_i}{\partial j} = 0$ for $i \neq j$, meaning that only the diagonal terms of the damping tensor are non-zero. Consequently, the damping rates in the x, y, and z directions simplify to:

$$\gamma_i = \frac{2\pi}{15m}\sigma R^5 \left(\frac{\partial B_i}{\partial i}\right)^2, \quad (i = x,y,z). \tag{5}$$

The applicability condition of Eq. (5) is that R is much smaller than the skin depth, $R \ll \delta = \sqrt{2/(\omega\sigma\mu)}$, where σ and μ represent the electrical conductivity and magnetic permeability, respectively. And the size of the metal sphere is much smaller than the magnetic field region of the levitation location, where the magnetic field gradient $\partial B_i/\partial i$ within the sphere can be approximated as uniform. For more details, see Supplementary Note 2. Since $m \propto R^3$, it follows that $\gamma_i \propto R^2$, indicating that smaller metal particles exhibit lower eddy current damping rates.

To verify the accuracy of our derived analytical expression Eq. (5), we first calculated the eddy current damping rate as a function of bismuth sphere diameter using the theoretical model, shown as the green line in Fig. 1a. Additionally, we employed finite element analysis (FEA) to simulate the eddy current damping rates of bismuth spheres with varying diameters; the simulation model is depicted in Fig. 1b, with a nominal bismuth sphere levitated in a diamagnetic trap. The simulation results are represented by purple red dots in Fig. 1a. A comparison between the simulation values and theoretical predictions showed a high degree of agreement, confirming the validity of the analytical expression Eq. (5). We then compared the eddy current damping rate with the air damping rate at a vacuum pressure of 1×10^{-6}mbar. The air damping rate, calculated using the empirical formula $16P/(\pi v R\rho)$, is illustrated by the orange line in Fig. 1a. A comparison between the green and orange lines reveals that the eddy current damping rate can theoretically be lower than the air damping rate for bismuth spheres with diameters smaller than the critical size of 5 μm, which varies with vacuum pressure (as described in Supplementary Note 3).

To reduce the eddy current damping rate, we conclude that using smaller levitated spheres results in lower eddy current damping. However, smaller spheres also have lower mass, which, according to Eq. (1), reduces their acceleration sensitivity. In many mass-related short-range force detection experiments, the sensor's acceleration sensitivity directly determines its ability to detect such forces. To address this issue, we propose replacing the monolithic bismuth sphere with a BM sphere. We hypothesize that the eddy current damping rate of the BM sphere primarily depends on the smaller particles that constitute it. Therefore, by using very small particles to form the BM sphere, we can achieve extremely low eddy current damping. At the same time, the BM sphere retains large mass. The combination of low eddy current damping and large mass is expected to greatly enhance its ability to detect short-range forces.

To test our hypothesis, we simulated and calculated the eddy current damping rate of a BM sphere and compared the results with those of a monolithic bismuth sphere of the same size. Fig. 1c shows the simulated eddy current damping for a monolithic bismuth sphere with a diameter of 0.8 mm, where the color bar represents the eddy current dissipation energy per unit volume. The simulation results indicate an eddy current damping rate of 0.244 Hz (consistent with the theoretical prediction from Eq. (5) with $2R = 0.8$ mm). At the same time, Fig. 1d presents the simulated results for a BM sphere with the same diameter, composed of 76.8 μm bismuth particles, yielding an eddy current damping rate of 2.26 mHz. This value is in good agreement with the theoretical prediction from Eq. (5), where $2R = 76.8$ μm. It is worth noting that we used a BM sphere constructed from 76.8 μm particles in the simulation to calculate the damping rate, rather than using

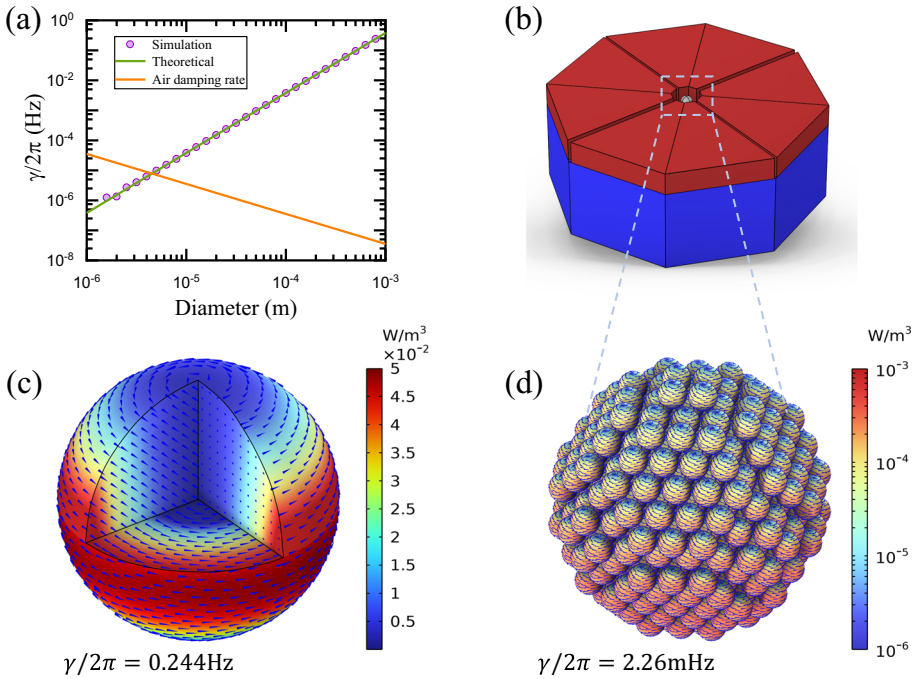

Fig. 1 | Theoretical model. a Damping rates vary with monolithic bismuth sphere's diameter. Purple red dots: FEA-simulated eddy current damping rate; Green line: our theoretical model predicted eddy current damping rate; Orange line: empirical formula calculated air damping rate at an air pressure of 1×10^{-6} mbar. **b** Simulation Model: a nominal bismuth sphere levitated in a diamagnetic trap composed of permanent magnets. The magnetic field gradient in the levitation region is $\partial B_z/\partial z = 1030$T/m according to the simulation. **c**, **d** Simulated distribution of eddy current dissipation energy per unit volume in two types of diamagnetically levitated bismuth spheres: (**c**) a monolithic bismuth sphere with a diameter of 0.8 mm; (**d**) a BM sphere with the same overall diameter, but composed of particles with diameters of 76.8 μm. Arrows in the spheres indicate the directions of the eddy currents, with the corresponding simulated eddy current damping values labeled at the bottom.

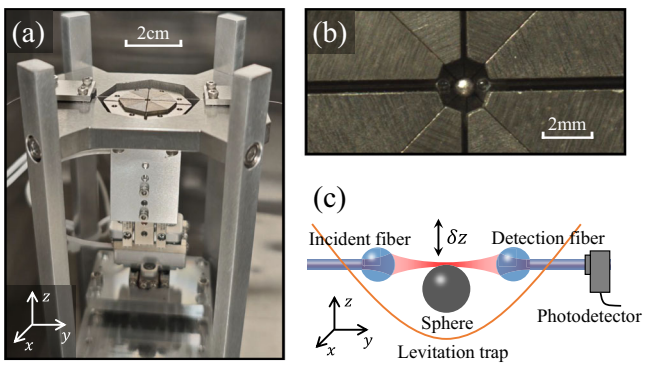

Fig. 2 | Experimental setup. a Photograph of the experimental setup. **b** Enlarged view of the levitation region: a manually polished bismuth sphere is levitated in the diamagnetic trap, with a pair of fused-ball fibers monitoring its displacement. **c** Schematic diagram illustrating the principle by which fused-ball fibers detect the displacement of the sphere: displacement is measured based on the sphere's obstruction of laser.

smaller particles that are closer to the following experimental size, due to computational hardware limitations. To determine the damping rate for a BM sphere constructed from smaller particles, we have theoretically derived that the eddy current damping rate of a BM sphere is solely determined by the size of the constituent particles and is independent of the overall size of the sphere, as detailed in the Methods section. Thus, we can calculate the damping rate of the BM sphere by using the damping rate of an individual particle, as given by Eq. (5).

Suppressing Eddy current damping by almost 1000-fold

To develop a levitated metal mechanical oscillator with high sensitivity, we experimentally fabricated the BM sphere proposed by our theoretical model. We investigated its damping rate, a key parameter that directly determines the oscillator's sensitivity, as described by Eq. (1). The experimental setup, shown in Fig. 2a, consists of a diamagnetic levitation trap, detection fibers, and a closed-loop motorized translation stage. The levitation trap comprises two layers of eight NdFeB magnets, forming a 2 mm-sized levitation region where a manually polished bismuth sphere is levitated, as illustrated in Fig. 2b. A 0.4 mm-wide slit between the magnets allows precise alignment of the detection fibers to monitor the sphere's displacement. The ends of the fibers are fused into 300 μm-diameter spheres (fused-ball fibers). A 1064 nm laser is focused by the fused ball at the incident fiber end, received by the fused ball at the detection fiber end, and converted into a voltage signal by a photodetector, as shown in Fig. 2c. As the sphere moves, it partially blocks the laser beam, causing changes in the detected laser power, which are used to measure the sphere's displacement. The coupling efficiency between the fibers exceeds 95%, demonstrating the high detection efficiency of the system. The entire setup is enclosed in a grounded permalloy electromagnetic shield to minimize electrical and magnetic interference, and a two-stage thermal isolation system made of PEEK columns reduces thermal fluctuations. The setup is housed in a vacuum chamber mounted on a commercial vibration isolation platform (Minus-K 850BM-1) to reduce seismic noise.

To quantify the sphere's displacement, the voltage signal from the photodetector was converted into displacement by determining the system's volt-meter coefficient. We focused on the sphere's motion along the z-axis. Using the closed-loop motorized translation stage, we adjusted the sphere's position relative to the detection fibers to maximize sensitivity to z-axis motion while minimizing responses in other directions. This position was established as the origin. The sphere was then displaced from this origin using the translation stage, and the corresponding displacements and photodetector voltages were recorded, as shown in Fig. 3a. Within the displacement range of $z = \pm 10\,\mu$m, the output voltage exhibited a linear response with a linearity of 0.997, and the slope of this line was defined as the volt-meter coefficient. All subsequent measurements of the sphere's motion were conducted within this validated linear range.

To validate the reliability of our experimental system, we first measured the damping rates of three monolithic bismuth spheres with diameters of 556 μm, 793 μm, and 1.05 mm, and examined the variation of their damping rates with diameter to assess consistency with the theoretical model described by Eq. (5). For each sphere, we recorded the displacement power spectral density (PSD) spectrum over a measurement duration of more than 10^4 s. The damping rates were determined by fitting a Lorentzian

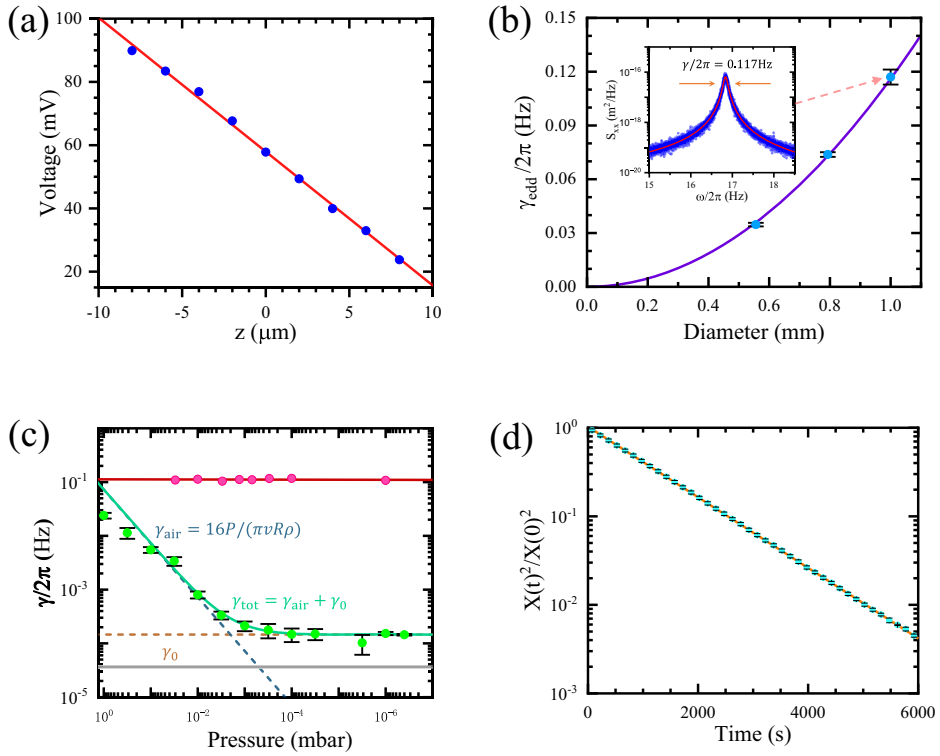

Fig. 3 | Damping rate measurements. a Linear response range of the photodetector output voltage as a function of sphere displacement. Blue dots represent the experimental values, and the red line is the fitted curve, with its slope indicating the volt-meter coefficient of the experimental setup. **b** Experimentally measured damping rates of three diamagnetically levitated monolithic bismuth spheres are shown as a function of their diameters. The sea blue dots represent the experimental data, the error bars were calculated as the standard deviation (s.d.) of the data, while the purple line represents the theoretical fitting curve based on Eq. (5). The fitting results indicate an actual magnetic field gradient of $\partial B_z/\partial z = 573$ T/m. Inset: Example of the measured power spectral density (PSD) for a 1.04 mm diameter monolithic bismuth sphere, measured over 10^4 s. The damping rate is determined from the half-width at half-maximum (HWHM) of the spectrum, obtained via Lorentzian fitting. **c** The damping rates of two types of diamagnetically levitated bismuth spheres as a function of pressure are shown: rose red for the 1.05 mm diameter monolithic bismuth sphere, and green for the 0.84 mm BM sphere. The rose red and green dots represent experimental data, with error bars for the green dots calculated as the s.d. of the data. The red solid line shows the fitted curve for the monolithic bismuth sphere. The dark blue dashed line represents the theoretical air damping rate (γ_{air}), while the brown dashed line corresponds to the fitted value of the final stabilized damping rate (γ_0) for the BM sphere. The green solid line represents the total damping rate (γ_{tot}), which is the sum of the air and stabilized damping rates. The gray line indicates the theoretically estimated eddy current damping rate for the BM sphere. **d** Ring-down curve of the 0.84 mm BM sphere at a pressure of 4×10^{-7} mbar, measured with 6000 s. The cyan dots represent the experimental values, with error bars indicating the s.d. of the data, while the orange line represents the fitted curve.

function to the PSD and extracting the full width at half maximum (FWHM). The experimental results are presented in Fig. 3b (sea blue dots). We used Eq. (5) to fit these data points, and the resulting fitting curve is shown as a purple line. With $\sigma = 8.7 \times 10^5$ S/m, the fitting process yields an actual magnetic field gradient of $\partial B_z/\partial z = 573$ T/m, which is smaller than the ideal value predicted in the simulation. Nevertheless, the close alignment between the experimental data and the theoretical fit confirms the reliability of the experimental system.

Next, we employed this experimental setup to measure the damping rate of a diamagnetically levitated BM sphere with a diameter of (0.84 ± 0.07) mm and a mass of (1.79 ± 0.03) mg. The BM sphere was fabricated by mixing vacuum glue with bismuth powder of (14.0 ± 10.8) μm in size. By substituting the bismuth powder size and the actual magnetic field gradient fitted from Fig. 3b into Eq. (5), we theoretically estimated the eddy current damping rate for the BM sphere to be (36.3 ± 0.3) μHz (See Supplementary Note 4), as represented by the gray line in Fig. 3c. The ring-down method was used to measure the damping rates at various vacuum pressures and compare them with those of a 1.05 mm diameter monolithic bismuth sphere. The results, shown in Fig. 3c, depict the experimental data for the monolithic bismuth sphere (rose red dots) and the BM sphere (green dots). The dark blue dashed line represents the theoretical value of air damping rate (γ_{air}), the brown dashed line corresponds to the fitted value of the final remnant damping rate (γ_0) of the BM sphere, and the green solid line is the sum of the two (γ_{tot}). The monolithic bismuth sphere exhibited a constant damping rate dominated by eddy currents across all measured vacuum pressures. In contrast, the BM sphere's damping rate decreased with decreasing vacuum pressure, until the vacuum pressure is decreased to 10^{-4} mbar. The remnant damping rate of the BM sphere is above the theoretical estimate. This will be addressed in the Discussion section. We also present the ring-down curve of the BM sphere at a vacuum pressure of 4×10^{-7} mbar, recorded over a 6000 s measurement period, as shown by the cyan dots in Fig. 3d. Fitting this curve with $X(t)^2 = X_0^2 e^{-\gamma t}$ revealed a damping rate as low as $\gamma_{tot}/2\pi = (144 \pm 6)$ μHz—almost three orders of magnitude lower than that of the monolithic bismuth sphere of the same size. With this ultra-low damping rate and the substantial mass of the BM sphere, its theoretical force sensitivity and acceleration sensitivity can reach $\sqrt{S_{FF}} = (5.17 \pm 0.12)\,\mathrm{fN}/\sqrt{\mathrm{Hz}}$ and $\sqrt{S_{aa}} = (0.30 \pm 0.01)\,\mathrm{ng}/\sqrt{\mathrm{Hz}}$, respectively, when in thermal equilibrium at room temperature (300 K). The main parameters in this experiment and the calculated sensitivities using these parameters are summarized in Table 1.

Application example

One important application of our diamagnetically levitated BM sphere will be to detect the gravitational force produced by a submilligram gravitational source. Detecting gravitational force between two small masses is a crucial step towards understanding the nature of gravity and exploring quantum gravity. Currently, the smallest detectable gravitational source was demonstrated by Westphal et al.[12] using a torsion balance-type detection

Table 1 | Summary of the main experimental parameters and the calculated sensitivities

Parameters	Symbol	value
Resonance fre.	$\omega_0/2\pi$	18.6 Hz
Diameter	$2R$	(0.84 ± 0.07)mm
Mass	m	(1.79 ± 0.03)mg
Density	ρ	(5.71 ± 1.45) × 10^3kg/m^3
Damping rate	$\gamma_{tot}/2\pi$	(144 ± 6) μHz
Q factor	Q	(1.29 ± 0.05) × 10^5
Force sensti.	$\sqrt{S_{ff}}$	(5.17 ± 0.12)fN/$\sqrt{\text{Hz}}$
Acceleration sensti.	$\sqrt{S_{aa}}$	(0.30 ± 0.01)ng/$\sqrt{\text{Hz}}$

Using a diamagnetically levitated BM sphere, all parameters were obtained at an ambient temperature of 300K and a vacuum pressure of 4 × 10^{-7}mbar.

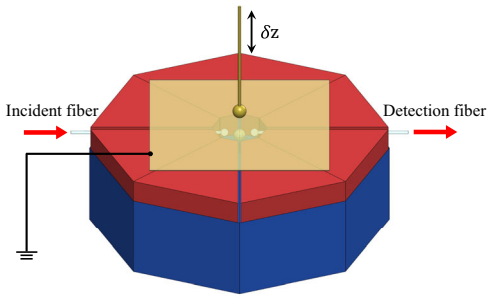

Fig. 4 | Proposed experimental setup to detect gravitational force. The diamagnetically levitated BM sphere serves as the test mass, and an oscillating submilligram gold sphere acts as the gravitational source. A pair of fused-ball fibers is aligned to detect the response displacement of the BM sphere, while a grounded metallic membrane is employed to shield electromagnetic interference between the two masses.

scheme to measure gravitational force between two 90 mg, 2 mm diameter gold spheres. To date, the gravitational force from masses below a milligram has never been experimentally measured.

Here, we propose using the diamagnetically levitated BM sphere as a test mass for submilligram gravitational force detection. The signal-to-noise ratio (SNR) for gravitational force detection can be expressed as:

$$\text{SNR} = \frac{Gmm_s/r^2}{\sqrt{S_{FF}\cdot b}} = \frac{Gm_s/r^2}{\sqrt{S_{aa}\cdot b}}, \tag{6}$$

where G is the gravitational constant, m and m_s are the masses of the test mass and gravitational source, respectively, r is the distance between their centers, $\sqrt{S_{FF}}$ and $\sqrt{S_{aa}}$ represent the force sensitivity and acceleration sensitivity of the diamagnetically levitated BM sphere, and $b = 1/t_{meas}$ is the measurement bandwidth. According to Eq. (1), S_{aa} is inversely proportional to m, meaning that a massive test mass improves the sensor's acceleration sensitivity. And for a given m, a higher density test mass leads to a smaller size, which reduces r and consequently enhances the SNR for a given m_s, as shown in Eq. (6). This is why metal mechanical oscillators hold an advantage in such force detection experiments.

The proposed experimental setup for detecting gravitational force produced by a submilligram source is shown in Fig. 4. A 1.79 mg, 0.84 mm diameter diamagnetically levitated BM sphere serves as the test mass, while a 0.9 mg, 0.45 mm diameter gold sphere functions as the gravitational source. The center-to-center distance between the two masses is set to $r = 1$ mm, and the gold sphere is periodically modulated along the z-axis at the resonance frequency, exerting a resonant gravitational acceleration of approximately 0.006 ng on the levitated BM sphere. With an acceleration sensitivity of $\sqrt{S_{aa}} = 0.3$ ng/$\sqrt{\text{Hz}}$, this setup is capable of detecting such a gravitational force between the two masses with a measurement time of $t_{meas} = 2500$ s, assuming SNR = 1.

To minimize external noise and optimize the system's sensitivity, we recommend placing a grounded metallic membrane between the two masses to effectively shield against electromagnetic interference[12]. Additionally, low-frequency seismic noise, a major source of disturbance, can be mitigated using a multi-stage spring isolation system[13].

Discussion

Developing a vacuum-levitated metal mechanical oscillator at room temperature with high sensitivity presents a promising avenue for advancing short-range force detection. In this article, we explore the feasibility of using a diamagnetic trap to levitate a metal mechanical oscillator. The system's stability is determined by the properties of permanent magnets and the high diamagnetic susceptibility of bismuth (-1.7×10^{-4}), making it an ideal material for levitation. Our experiments successfully demonstrated stable levitation of bismuth spheres across a wide size range, from micrometers to millimeters, particularly suited for short-range force detection.

However, the performance of levitated metal systems is limited by eddy current damping, which significantly impacts the system's sensitivity. To address this issue, we designed a bismuth micro-particles constructed sphere (BM sphere) and theoretically derived its eddy current damping rate formula. The results show that the damping rate is primarily determined by the micro-particles' size. We prepared the BM sphere using bismuth powder with particle sizes of (14.0 ± 10.8) μm. Theoretical estimations indicated that its eddy current damping rate should be (36.3 ± 0.3) μHz under the current experimental conditions. However, the experimentally measured remnant eddy current damping rate reached (144 ± 6) μHz. We speculate that this discrepancy may stem from several factors: the non-uniform size distribution of the bismuth powder particles, possible energy dissipation caused by surface charges on the BM sphere[45], magnetic field fluctuations induced by the motion of the BM sphere, and eddy current losses potentially arising from particle-to-particle contact. Further details of this analysis can be found in Supplementary Note 4. To address these issues, future work will focus on optimizing the size and distribution of the bismuth powder particles and employing ultraviolet light to discharge the BM sphere, thereby reducing the interference caused by induced charges. These improvements are expected to further lower the mechanical damping rate and enhance the overall sensitivity of the system.

Despite this, our experimental results demonstrated that the BM sphere achieved an ultra-low damping rate of $\gamma_{tot}/2\pi = (144 \pm 6)\ \mu Hz$, nearly three orders of magnitude lower than that of a monolithic bismuth sphere of equivalent size. To the best of our knowledge, this is the first instance of achieving such a low mechanical damping rate with a metal mechanical oscillator at room temperature. Using these experimental parameters, we calculated that the levitated BM sphere can exhibit impressive force sensitivity of (5.17 ± 0.12) fN/$\sqrt{\text{Hz}}$ and acceleration sensitivity of (0.30 ± 0.01) ng/$\sqrt{\text{Hz}}$ under thermal equilibrium, underscoring its potential for high-precision short-range force detection.

Looking ahead, this levitated BM sphere can be suitable for detecting gravitational force produced by submilligram masses, a challenge that remains beyond the capabilities of existing precision measurement techniques. Currently, our system's performance is constrained by low-frequency seismic noise of 6 ng/$\sqrt{\text{Hz}}$@18.6Hz (See Supplementary Note 5), preventing it from reaching thermal equilibrium. To overcome this, we plan to implement multi-stage spring isolation, a well-established technique that can reduce platform vibrations to 0.3 ng/$\sqrt{\text{Hz}}$[13]. Once implemented, this isolation is expected to enable the system to achieve the sensitivity necessary for detecting gravitational interactions from submilligram masses, opening new possibilities for precision measurements and the exploration of fundamental forces.

Methods

Preparation of the BM sphere

We created the BM sphere prototype by mixing bismuth powder (with particle sizes of (14.0 ± 10.8) μm) with vacuum glue. After the vacuum glue naturally air-dried, we manually polished it into a spherical shape of the desired size. The spheres were then cleaned with alcohol, polished with frosted glass, and finally placed in an oven at 80 °C for 3 h. The finished samples were subsequently levitated in a diamagnetic trap.

Finite element analysis (FEA)

We used the magnetic and electric fields (mef) module in COMSOL Multiphysics simulation software to simulate the magnetic field distribution within the diamagnetic trap. We further simulated the eddy currents induced in the bismuth sphere as it moved through the magnetic field. The parameters used for the bismuth sphere in the simulation include electrical conductivity $\sigma = 8.7 \times 10^5$ S/m, density $\rho = 9.8 \times 10^3$ kg/m^3, and magnetic susceptibility $\chi = -1.7 \times 10^{-4}$. By assigning a specific velocity to the bismuth sphere, we simulated the Lorentz force per unit volume acting on the sphere. This force was then integrated over the entire volume of the bismuth sphere to obtain the net Lorentz force in each direction, corresponding to the total damping force. Finally, by calculating the relationship between the damping force and the velocity in each direction, we determined the eddy current damping rate γ_{ij}.

For the BM sphere simulation, we constructed a bismuth sphere with a diameter of 0.4 mm, composed of 490 smaller spheres, each with a diameter of 76.8 μm, arranged in a close-packed structure (as shown in Fig. 1d). We then simulated the eddy current damping rates for both the BM sphere and a monolithic sphere of the same overall size. The damping rates were found to be 2.23 mHz for the BM sphere and 0.244 Hz for the monolithic sphere, indicating that the BM sphere's damping rate is two orders of magnitude smaller. Furthermore, we simulated that a monolithic sphere of 76.8 μm diameter has an eddy current damping rate of 2.26 mHz, which closely matches that of the BM sphere. This demonstrates that the eddy current damping rate of the BM sphere is primarily determined by the damping rate of its constituent particles, rather than by the overall size of the bismuth sphere. This can also be analytically proven: let the BM sphere consist of N small particles, each with mass m and an individual eddy current damping rate γ_s. Neglecting the mass of the glue, the total mass of the BM sphere is $M = Nm$. The total eddy current damping force of the BM sphere can be expressed as:

$$F_{\mathrm{BM}} = NF_s = Nm\gamma_s v = M\gamma_s v, \tag{7}$$

where $F_s = m\gamma_s v$ is the eddy current damping force for an individual small particle. Therefore, the eddy current damping rate of the BM sphere is:

$$\gamma_{\mathrm{BM}} = \frac{F_{\mathrm{BM}}}{Mv} = \gamma_s, \tag{8}$$

this shows that the BM sphere's eddy current damping rate is equal to the damping rate of its constituent small particles. In practice, considering the mass of the glue, the overall eddy current damping rate of the BM sphere is slightly lower than that of an individual small particle.

Data availability

The experimental data for all figures in the main text of this work are provided in Supplementary Data 1. Other data that support the findings of this study are available from the corresponding author upon request.

Code availability

The simulation code that supports the plots within this paper is available from the corresponding author upon reasonable request.

Received: 13 October 2024; Accepted: 18 February 2025;
Published online: 26 February 2025

References

1. Lamoreaux, S. K. The Casimir force: background, experiments, and applications. *Rep. Prog. Phys.* **68**, 201 (2004).
2. Mitrofanov, V. & Ponomareva, I. Experimental test of gravitation at small distances. *Zh. Eksp. Teor. Fiz.* **94**, 16–22 (1988).
3. Long, J. C., Chan, H. W. & Price, J. C. Experimental status of gravitational-strength forces in the sub-centimeter regime. *Nucl. Phys. B* **539**, 23–34 (1999).
4. Moody, J. & Wilczek, F. New macroscopic forces? *Phys. Rev. D.* **30**, 130 (1984).
5. Long, J. C. et al. Upper limits to submillimetre-range forces from extra space-time dimensions. *Nature* **421**, 922–925 (2003).
6. Bertolini, S., Di Luzio, L. & Nesti, F. Axion-mediated forces, *cp* violation, and left-right interactions. *Phys. Rev. Lett.* **126**, 081801 (2021).
7. Sugimoto, Y. et al. Chemical identification of individual surface atoms by atomic force microscopy. *Nature* **446**, 64–67 (2007).
8. Harris, B., Chen, F. & Mohideen, U. Precision measurement of the casimir force using gold surfaces. *Phys. Rev. A* **62**, 052109 (2000).
9. Klimchitskaya, G., Mohideen, U. & Mostepanenko, V. The casimir force between real materials: Experiment and theory. *Rev. Mod. Phys.* **81**, 1827–1885 (2009).
10. Kim, W.-J., Sushkov, A., Dalvit, D. A. & Lamoreaux, S. Surface contact potential patches and casimir force measurements. *Phys. Rev. A-At., Mol., Optical Phys.* **81**, 022505 (2010).
11. Ke, J. et al. Combined test of the gravitational inverse-square law at the centimeter range. *Phys. Rev. Lett.* **126**, 211101 (2021).
12. Westphal, T., Hepach, H., Pfaff, J. & Aspelmeyer, M. Measurement of gravitational coupling between millimetre-sized masses. *Nature* **591**, 225–228 (2021).
13. Fuchs, T. M. et al. Measuring gravity with milligram levitated masses. *Sci. Adv.* **10**, eadk2949 (2024).
14. Lee, J. G., Adelberger, E. G., Cook, T. S., Fleischer, S. M. & Heckel, B. R. New test of the gravitational $1/r^2$ law at separations down to 52μm. *Phys. Rev. Lett.* **124**, 101101 (2020).
15. Arvanitaki, A. & Geraci, A. A. Resonantly detecting axion-mediated forces with nuclear magnetic resonance. *Phys. Rev. Lett.* **113**, 161801 (2014).
16. Gao, D. Z. et al. Using metallic noncontact atomic force microscope tips for imaging insulators and polar molecules: tip characterization and imaging mechanisms. *ACS nano* **8**, 5339–5351 (2014).
17. Geraci, A. A., Smullin, S. J., Weld, D. M., Chiaverini, J. & Kapitulnik, A. Improved constraints on non-newtonian forces at 10 microns. *Phys. Rev. D.* **78**, 022002 (2008).
18. Chen, Y.-J. et al. Stronger limits on hypothetical yukawa interactions in the 30–8000 nm range. *Phys. Rev. Lett.* **116**, 221102 (2016).
19. Vinante, A., Mezzena, R., Falferi, P., Carlesso, M. & Bassi, A. Improved noninterferometric test of collapse models using ultracold cantilevers. *Phys. Rev. Lett.* **119**, 110401 (2017).
20. Hoskins, J., Newman, R., Spero, R. & Schultz, J. Experimental tests of the gravitational inverse-square law for mass separations from 2 to 105 cm. *Phys. Rev. D.* **32**, 3084 (1985).
21. Tan, W.-H. et al. New test of the gravitational inverse-square law at the submillimeter range with dual modulation and compensation. *Phys. Rev. Lett.* **116**, 131101 (2016).
22. Kapner, D. J. et al. Tests of the gravitational inverse-square law below the dark-energy length scale. *Phys. Rev. Lett.* **98**, 021101 (2007).
23. Hoedl, S. A., Fleischer, S. M., Adelberger, E. G. & Heckel, B. R. Improved constraints on an axion-mediated force. *Phys. Rev. Lett.* **106**, 041801 (2011).
24. Millen, J., Monteiro, T. S., Pettit, R. & Vamivakas, A. N. Optomechanics with levitated particles. *Rep. Prog. Phys.* **83**, 026401 (2020).
25. Gonzalez-Ballestero, C., Aspelmeyer, M., Novotny, L., Quidant, R. & Romero-Isart, O. Levitodynamics: Levitation and control of microscopic objects in vacuum. *Science* **374**, eabg3027 (2021).

26. Jin, Y., Shen, K., Ju, P. & Li, T. Towards real-world applications of levitated optomechanics. *arXiv preprint arXiv:2407.12496* (2024).
27. Ranjit, G., Cunningham, M., Casey, K. & Geraci, A. A. Zeptonewton force sensing with nanospheres in an optical lattice. *Phys. Rev. A* **93**, 053801 (2016).
28. Shan, X. et al. Sub-femtonewton force sensing in solution by super-resolved photonic force microscopy. *Nat. Photonics* **18**, 913–921 (2024).
29. Monteiro, F., Ghosh, S., Fine, A. G. & Moore, D. C. Optical levitation of 10-ng spheres with nano-*g* acceleration sensitivity. *Phys. Rev. A* **96**, 063841 (2017).
30. Prat-Camps, J., Teo, C., Rusconi, C., Wieczorek, W. & Romero-Isart, O. Ultrasensitive inertial and force sensors with diamagnetically levitated magnets. *Phys. Rev. Appl.* **8**, 034002 (2017).
31. Qvarfort, S., Serafini, A., Barker, P. F. & Bose, S. Gravimetry through non-linear optomechanics. *Nat. Commun.* **9**, 3690 (2018).
32. Timberlake, C., Gasbarri, G., Vinante, A., Setter, A. & Ulbricht, H. Acceleration sensing with magnetically levitated oscillators above a superconductor. *Appl. Phys. Lett.* **115**, 224101 (2019).
33. Lewandowski, C. W., Knowles, T. D., Etienne, Z. B. & D'Urso, B. High-sensitivity accelerometry with a feedback-cooled magnetically levitated microsphere. *Phys. Rev. Appl.* **15**, 014050 (2021).
34. Omine, R., Masui, S., Kadoya, S., Michihata, M. & Takahashi, S. Manipulation of large, irregular-shape particles using contour-tracking optical tweezers. *Opt. Lett.* **49**, 2773–2776 (2024).
35. Būtaitė, U. G. et al. Photon-efficient optical tweezers via wavefront shaping. *Sci. Adv.* **10**, eadi7792 (2024).
36. Brandt, E. Levitation in physics. *Science* **243**, 349–355 (1989).
37. Hofer, J. & Aspelmeyer, M. Analytic solutions to the maxwell–london equations and levitation force for a superconducting sphere in a quadrupole field. *Phys. Scr.* **94**, 125508 (2019).
38. Ge, S. et al. Magnetic levitation in chemistry, materials science, and biochemistry. *Angew. Chem. Int. Ed.* **59**, 17810–17855 (2020).
39. Vinante, A. et al. Ultralow mechanical damping with meissner-levitated ferromagnetic microparticles. *Phys. Rev. Appl.* **13**, 064027 (2020).
40. Hofer, J. et al. High-*q* magnetic levitation and control of superconducting microspheres at millikelvin temperatures. *Phys. Rev. Lett.* **131**, 043603 (2023).
41. Yin, P. et al. Experiments with levitated force sensor challenge theories of dark energy. *Nat. Phys.* **18**, 1181–1185 (2022).
42. Chen, X., Ammu, S. K., Masania, K., Steeneken, P. G. & Alijani, F. Diamagnetic composites for high-q levitating resonators. *Adv. Sci.* **9**, 2203619 (2022).
43. Xie, H. et al. Suppressing mechanical dissipation of diamagnetically levitated oscillator via engineering conductive geometry. *Phys. Rev. Res.* **5**, 013030 (2023).
44. Tian, S. et al. Feedback cooling of an insulating high-q diamagnetically levitated plate. *Appl. Phys. Lett.* **124**, 124002 (2024).
45. Zhu, X. et al. Suppression of damping in a diamagnetically levitated dielectric sphere via eddy currents and static charge reduction. *Opt. Express* **31**, 34493–34502 (2023).

Acknowledgements

I would like to thank Professor Pu Huang from Nanjing University for his valuable suggestions on this paper. This work was supported by the fellowship of China Postdoctoral Science Foundation (Grant No. 2022TQ0314) and Key R&D Program of Zhejiang (2024SSYS0014, 3000-3AA240100).

Author contributions

All authors contributed to the development and writing of this paper. Tong Wu conceived the general idea, performed theoretical calculations, and drove the overall progress of the work. Cuihong Li supervised the experiment and provided some financial support for the experiments. Fang Xiong designed and built the experimental setup, and drafted the manuscript. Leilei Guo was responsible for the fabrication of mechanical components. Zhiming Chen provided guidance on vacuum operations. Aimin Du contributed valuable suggestions during the manuscript revision process and participated in the revision of the paper.

Competing interests

The authors declare no competing interests.

Additional information

Supplementary information The online version contains supplementary material available at https://doi.org/10.1038/s42005-025-02010-7.

Correspondence and requests for materials should be addressed to Cuihong Li or Tong Wu.

Peer review information *Communications Physics* thanks the anonymous reviewers for their contribution to the peer review of this work. A peer review file is available.